Stem Cell Research 27 (2018) 151–161

Contents lists available at ScienceDirect

Stem Cell Research

journal homepage: www.elsevier.com/locate/scr

Effect of prolonged differentiation on functional maturation of human pluripotent stem cell-derived neuronal cultures

Tanja Paavilainen [a,1], Anssi Pelkonen [a,1], Meeri E.-L. Mäkinen [a], Marja Peltola [a], Heini Huhtala [b], Dmitriy Fayuk [a], Susanna Narkilahti [a,*]

[a] NeuroGroup, BioMediTech and Faculty of Medicine and Life Sciences, University of Tampere, Arvo Ylpön katu 34, 33520 Tampere, Finland
[b] Faculty of Social Sciences, University of Tampere, Arvo Ylpön katu 34, 33520 Tampere, Finland

ARTICLE INFO

Article history:
Received 10 November 2017
Received in revised form 9 January 2018
Accepted 17 January 2018
Available online 31 January 2018

Keywords:
Astrocytes
Calcium signaling
Microelectrode array
Neural development
Neurons
Pluripotent stem cells

ABSTRACT

Long-term neural differentiation of human pluripotent stem cells (hPSCs) is associated with enhanced neuronal maturation, which is a necessity for creation of representative *in vitro* models. It also induces neurogenic-to-gliogenic fate switch, increasing proportion of endogenous astrocytes formed from the common neural progenitors. However, the significance of prolonged differentiation on the neural cell type composition and functional development of hPSC-derived neuronal cells has not been well characterized. Here, we studied two hPSC lines, both of which initially showed good neuronal differentiation capacity. However, the propensity for endogenous astrogenesis and maturation state after extended differentiation varied. Live cell calcium imaging revealed that prolonged differentiation facilitated maturation of GABAergic signaling. According to extracellular recordings with microelectrode array (MEA), neuronal activity was limited to fewer areas of the culture, which expressed more frequent burst activity. Efficient maturation after prolonged differentiation also promoted organization of spontaneous activity by burst compaction. These results suggest that although prolonged neural differentiation can be challenging, it has beneficial effect on functional maturation, which can also improve transition to different neural *in vitro* models and applications.

1. Introduction

Human pluripotent stem cell (hPSC)-derived neurons hold a great promise for modeling neurodevelopment as well as pathologies with genetic background (Suzuki and Vanderhaeghen, 2015). Additionally, hPSC-derived neuronal cultures represent a promising platform for neurotoxicity testing (Johnstone et al., 2010; Ylä-Outinen et al., 2010) and a therapy option, for example, in Parkinson's disease and spinal cord injury (Li et al., 2015; Lindvall, 2015). hPSCs include human embryonic stem cells (hESCs) (Thomson, 1998) and human induced pluripotent stem cells (hiPSCs) (Takahashi et al., 2007), both of which have their advantages and disadvantages. hESCs are considered to have fewer obstacles to differentiation because they do not carry any previous epigenetic memory of former cellular identity (Kim et al., 2010), whereas hiPSCs are associated with fewer ethical problems and wider utilization potential in applications such as modeling of hereditary diseases (Du and Parent, 2015). hPSCs can be differentiated into spontaneously active functional neuronal networks (Heikkilä et al., 2009; Toivonen et al., 2013), but to gain greater benefits from hPSC-derived neural cells for various applications, their basic characteristics need to be studied and evaluated in more detail *in vitro*, especially at the level of functional development.

Achieving functional maturation of hPSC-derived neuronal cells *in vitro* still remains a challenge in the field. When compared to rodent primary neurons, the functional state of hPSC-derived neuronal cultures can be considered immature. Traditionally, the survival in long-term culture and functional maturation of hPSC-derived neural cultures has been enhanced with primary rodent astrocytes in cocultures (Frega et al., 2017; Johnson et al., 2007; Odawara et al., 2014). After all, astrocytes have been recognized as active regulators of neuronal development and function (Clarke and Barres, 2013). However, for most hPSC-derived neuronal applications, for example disease modeling, a completely human cell-based system is a necessity. At the same time many differentiation protocols for hPSC-derived neurons typically produce a varying proportion of astrocytes from the common neural progenitors (Lappalainen et al., 2010; Pasca et al., 2015; Shi et al., 2012). Still this change in cell type composition is not often discussed. Overall, the significance of prolonged differentiation on neural cell type composition and network level functional studies describing this development are still largely lacking.

Here, we describe how prolonged neural differentiation affects the generation of endogenous astrocytes and impacts the functional

* Corresponding author.
E-mail address: susanna.narkilahti@uta.fi (S. Narkilahti).
[1] These authors contributed equally to this work.

https://doi.org/10.1016/j.scr.2018.01.018

development of hPSC-derived neural cultures. Typically, extended differentiation of hPSC-derived neurons is supported by rodent astrocyte coculture but here only hPSC-derived cultures were used. Our neurosphere differentiation method recapitulates the *in vivo* developmental stages in which the switch from neurogenesis to gliogenesis occurs over time (Lappalainen et al., 2010; Miller and Gauthier, 2007; Zhang et al., 2001). Accordingly, we selected two time points of neurosphere differentiation, the standard 8 week and the prolonged 15 week time point, which were quantitatively analyzed for neuronal and astrocytic markers using immunocytochemistry and gene expression analysis. Microelectrode array (MEA) technique was used to measure spontaneous electrical activity repeatedly in large populations of neurons. In contrast, calcium (Ca^{2+}) imaging allowed detection of individual cell type specific activity in neurons and astrocytes. Together, Ca^{2+} imaging and MEA system were validated as useful tools in providing extensive information about hPSC-derived neural cultures, and indicated functional maturation of neuronal cells after prolonged differentiation.

2. Materials and methods

2.1. Maintenance of human pluripotent stem cells

The human embryonic stem cell (hESC) line Regea 08/023 (passages 14–66) and the human induced pluripotent stem cell (hiPSC) line 04311.WT (passages 24–45) were used in this study. The cell lines were derived at the Institute of Biosciences and Medical Technology (BioMediTech), University of Tampere, Finland. BioMediTech received approval from the Finnish Medicines Agency (FIMEA) to perform research using human embryos (Dnro 1426/32/300/05). Supportive statements were also obtained from the regional ethics committee of Pirkanmaa Hospital District for the derivation, culture, and differentiation of hESCs (R05116) and hiPSCs (R08070). An informed consent was obtained from all subjects who provided cell samples. All methods were carried out in accordance with relevant guidelines and regulations. The hESC line Regea 08/023 was generated as previously described (Rajala et al., 2010; Skottman, 2010). The hiPSC line 04311.WT was derived from human skin fibroblasts following a previously published protocol using Sendai virus technology (Ojala et al., 2016) (Supplementary Fig. 1). The hPSC-lines were cultured on top of a human feeder cell layer (CRL-2429, ATCC, Manassas, VA, USA) and were passaged weekly (Rajala et al., 2007). The medium consisted of knockout Dulbecco's modified Eagle's medium (DMEM) supplemented with 20% knockout serum replacement, 2 mM Glutamax (all from Gibco, Thermo Fisher Scientific Waltham, MA USA), 1% nonessential amino acids, 50 U ml^{-1} penicillin/streptomycin (both from Lonza Group Ltd., Basel, Switzerland), 0.1 mM 2-mercaptoethanol (Gibco, Thermo Fisher Scientific) and 8 ng ml^{-1} basic fibroblast growth factor (bFGF, R&D Systems Inc., Minneapolis, MN, USA). The undifferentiated stage of both human pluripotent stem cell (hPSC) lines were regularly monitored with gene and protein expression analyses of pluripotency markers (Nanog, Oct-3/4, TRA-1-81 and TRA-1-60) and markers for different germ layers (human alpha-smooth muscle actin, human alpha-fetoprotein, and Nestin). All cultures maintained normal karyotypes and were mycoplasma free.

2.2. Neural differentiation

Neural differentiation of hESCs (Regea 08/023) and hiPSCs (04311.WT) was performed using a free-floating neurosphere culture (Lappalainen et al., 2010). hPSC colonies were mechanically cut into small clusters and transferred into six-well ultra-low attachment plates (Nunc, Thermo Fisher Scientific) for neural differentiation. Neural differentiation medium (NDM) consisted of 1:1 DMEM/F-12:Neurobasal medium supplemented with 1× B27, 1× N2, and 2 mM Glutamax (all from Gibco, Thermo Fisher Scientific), 25 U ml^{-1} penicillin/streptomycin (Lonza Group Ltd.) and 20 ng ml^{-1} bFGF (R&D Systems Inc.). The medium was changed three times per week, and the neurospheres were mechanically passaged once per week. Cells were differentiated in neurosphere culture for standard 8 weeks or prolonged 15 weeks and plated under adherent culture conditions for maturation up to 5 weeks (Fig. 1A, experimental setup). For adherent culture the neurospheres were mechanically cut into small 50–200 μm in diameter clusters containing on average 5000–10,000 cells. The number of plated clusters was relative to culture area: 10 clusters for MEA experiments, 20 clusters for calcium imaging experiments, 20 clusters for immunocytochemistry and PCR experiments. Cells were plated either on glass coverslips or MEA dishes coated with 0.05% PEI and 20 μg ml^{-1} mouse laminin (both from Sigma-Aldrich, St. Louis, MO, USA). For adherent culture bFGF was omitted from the NDM. After one week of adherent culture, 4 ng ml^{-1} bFGF and 5 ng ml^{-1} brain-derived neurotrophic factor (BDNF, Prospec, Rehovot, Israel) were added to the NDM to support neuronal maturation. The cultures were maintained with three medium changes per week.

2.3. Immunocytochemistry

Protein expression in cultures was characterized with immunocytochemical staining as previously described (Lappalainen et al., 2010). The following primary antibodies were used: MAP-2 (rabbit, 1:400, Millipore, Billerica, MA, USA: AB5622), MAP-2 (chicken, 1:4000, Novus Biologicals, Littleton, CO, USA: NB300-213), β_{III}-tubulin (rabbit, 1:2000, GenScript, Piscataway, NJ, USA: A01627), β_{III}-tubulin (chicken, 1:4000, Abcam, Cambridge, MA, USA: ab107216), GFAP (chicken, 1:4000, Abcam: ab4674), synaptophysin (mouse, 1:2000, Sigma-Aldrich: s5768), vGlut (guinea pig, 1:1000, Millipore: AB2251), GABA (rabbit, 1:1000, Sigma-Aldrich: A2052), GAD67 (mouse, 1:100, Millipore: MAB5406), TH (mouse, 1:800, Sigma-Aldrich: T1299), serotonin (rabbit, 1:800, Sigma-Aldrich: S5545), and S100β (mouse, 1:500, Abcam: ab11178). For secondary antibody labeling, Alexa Fluor 488 (1:400), Alexa Fluor 568 (1:400) or Alexa Fluor 647 (1:200) dye (Thermo Fisher Scientific) was used as appropriate. The cells were imaged using an Olympus IX51 microscope (10×, NA = 0.3 and 20×, NA = 0.45 objectives) equipped with an Olympus DP30BW camera (Olympus Corporation, Hamburg, Germany). For synaptophysin staining, an LSM780 Laser Scanning Confocal Microscope (40× objective, NA = 1.4) with a Quasar spectral GaAsP detector (all from Carl Zeiss, Jena, Germany) was used.

To quantify the neuron-to-astrocyte ratio at the 8 and 15 wk. time points, cells were plated under adherent culture conditions and were stained after 2 and 4 wks for neuronal (MAP-2 + β-tubulin) and astrocyte (GFAP) markers. The numbers of biological and technical repeats are listed in Supplementary Table 2. Distinct cell types were automatically counted using CellProfiler (Carpenter et al., 2006) and CellProfiler Analyst (Jones et al., 2008) software. The results of the automated analysis were evaluated manually, and samples with fewer than 200 cells or a false classification result were excluded from the final analysis.

2.4. RT-PCR analysis and qRT-PCR array

Total RNA was isolated from 8 + 5 wks and 15 + 5 wks differentiated cells using the NucleoSpin RNA XS kit (Macherey-Nagel, Düren, Germany) according to the manufacturer's instructions. The concentration and quality of the RNA were monitored spectroscopically. For each sample, 800 ng of total RNA was reverse transcribed into cDNA with the High Capacity cDNA Reverse Transcription kit (Applied Biosystems, Thermo Fisher Scientific, Foster City, CA, USA) according to the manufacturer's instructions.

To investigate brain region specificity and chloride transporter expression, a standard RT-PCR analysis was performed (target genes, primer sequences and exact annealing temperatures in Supplementary Table 1). For each reaction, an aliquot of 2.5 ng cDNA was used with

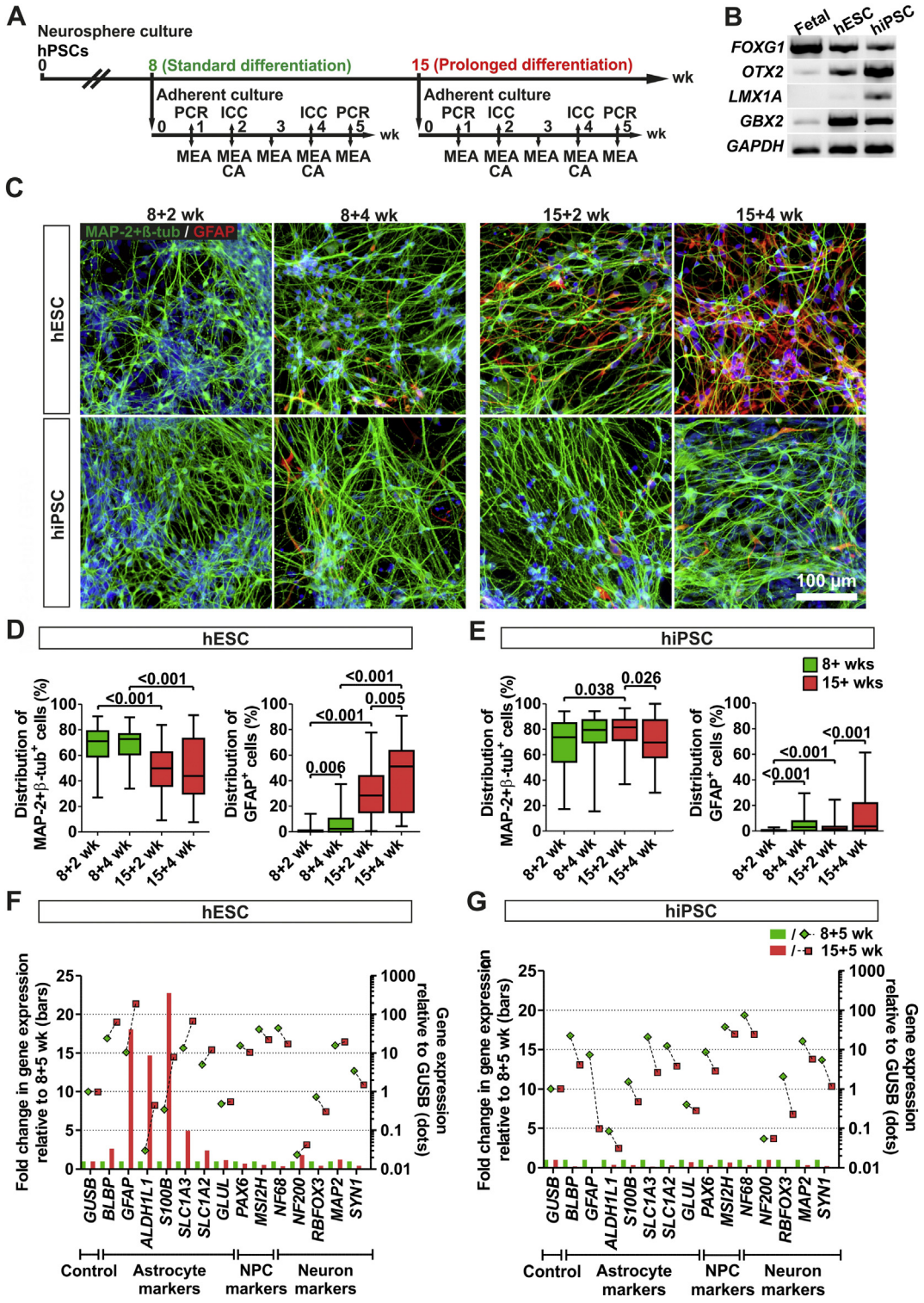

Fig. 1. Differentiation of hESC- and hiPSC-derived neurons and astrocytes. (A) hPSCs were first differentiated in neurosphere culture for 8 or 15 wks and then plated under adherent culture conditions for maturation up to five weeks before characterization with immunocytochemical staining (ICC), PCR, Ca^{2+} imaging (CA), and microelectrode array (MEA). (B) At 8 + 1 wk. time point RNA was extracted from cultures and RT-PCR was performed for forebrain (*FOXG1* and *OTX2*), midbrain (*LMX1A*) and hindbrain markers (*GBX2*) ($n = 1$). Human fetal brain RNA was used as control. The displayed bands were cropped from a single image of one gel (Supplementary Fig. 5A). (C) Representative images of immunocytochemical staining of neuronal (MAP-2 + β-tubulin) and astrocyte (GFAP) markers after standard (8+ wks) and prolonged (15+ wks) differentiation. 4′,6-diamidino-2-phenylindole (DAPI) nuclear staining is in blue. (D, E) The percentages of neurons and astrocytes were counted using CellProfiler analysis tools. The data are presented as the distribution of the percentages of neurons and astrocytes at each time point. The median and interquartile ranges are indicated by lines, and the whiskers indicate the minimum and maximum of the data. A non-parametric Mann-Whitney *U* test was used for the statistical analysis, and p-values <0.05 were considered significant. Significant p-values are presented in the images. The number of samples analyzed is presented in Supplementary Table 2. (F, G) At the 8 + 5 and 15 + 5 wk. time points, qPCR was performed to evaluate various neural precursor cell (NPC) markers and markers of mature neurons and astrocytes (n = 1, 3 technical replicates). The bars represent the fold change in gene expression between 8 + 5 and 15 + 5 wks, and they correspond to the left *y*-axis. The dots indicate the variable expression levels of genes compared to the housekeeping gene *GUSB*, and they correspond to the right *y*-axis (logarithmic).

0.2 mM of both forward and reverse primers, 1 × PCR buffer (–MgCl, + KCl), 1.5 mM $MgCl_2$, 0.1 mM dNTP mix and 0.25 U/μl Taq DNA polymerase (Qiagen, Hilden, Germany). The cDNA was amplified using 37 PCR cycles with an initializing step at 95 °C for 3 min, DNA denaturation at 95 °C for 30 s, annealing at 60–68 °C (Supplementary Table 1) for 30 s and elongation at 72 °C for 1 min. A 5 min elongation step finalized the reaction. The PCR products were separated electrophoretically on a 1.5% agarose gel in Tris/Borate/EDTA buffer containing GelRed (Biotium, Hayward, CA, USA) and visualized using BioRad ChemiDoc MP system (Bio-rad Laboratories, Inc., Hercules, CA, USA).

To investigate astrocyte, neural precursor and general neuron genes, a gene expression array analysis of a subset of 14 genes of interest (Supplementary Table 1) was performed using a custom TaqMan® Array (Applied Biosystems) according to the manufacturer's instructions. For each reaction, 6 ng of cDNA was used with TaqMan® Universal PCR Master Mix (Applied Biosystems). The analysis was performed using the ABI Prism 7300 real-time PCR system (Applied Biosystems). The data were normalized to the expression of the housekeeping gene GUSB, and the data from the 15 + 5 wks time point were further compared to the 8 + 5 wks time point. Relative expression values were determined using the comparative $2^{-\Delta\Delta Ct}$ method, and the quality of the PCR products was monitored with a melt curve analysis. The analysis consisted of three technical replicates.

2.5. Ca^{2+} imaging

Ca^{2+} signaling of 8 and 15 weeks differentiated cells was studied after 2 and 4 wks of adherent maturation. Cells were loaded with 4 μM of Fluo-4 AM (Thermo Fisher Scientific) diluted in NDM for 30 min at 37 °C and 5% CO_2, followed by washing with NDM for another 30 min at 37 °C and 5% CO_2. Culture were imaged every 0.5 s while being continuously perfused with physiological solution at 36 ± 0.5 °C at a rate of 2 ml/min (RC-22 perfusion chamber, TC-344C temperature controller, SH-27B in-line solution heater; Warner Instruments Inc., Hamden, USA). The physiological solution contained 140 mM NaCl, 10 mM HEPES, 10 mM D-glucose, 3.5 mM KCl, 1.25 mM NaH_2PO_4, 2 mM $CaCl_2$ and 1 mM $MgCl_2$ (all from Sigma-Aldrich) dissolved in dH_2O. The fluorescent imaging system consisted of an Olympus IX61 inverted microscope (10× and 20× objectives, NA = 0.5), an Andor iXon 885 EMCCD camera (Andor Technology, Belfast, Northern Ireland) and a Polychrom V monochromator (TILL Photonics, Munich, Germany). Images were acquired with TILL Photonics Live Acquisition software and analyzed with SimplePCI software package (Hamamatsu Corporation, Sewickley, PA, USA). Neuronal cells were identified by their morphology and ability to quickly respond to elevated extracellular K^+ (50 mM). Ca^{2+} signaling was considered related to action potentials if it was blocked by the voltage-gated sodium channel antagonist tetrodotoxin (TTX, 1 μM, Tocris Bioscience, Bristol, UK). GABA (100 μM, Sigma-Aldrich) and glutamate (50 μM, Sigma-Aldrich) were applied to test for the presence of functional receptors for these major neurotransmitters. The fluorescence intensity was normalized to the resting level, and amplitude of the GABA and glutamate responses in each cell was calculated as a fraction of the response to high-K^+ depolarization in the cell. The numbers of biological and technical repeats are listed in Supplementary Table 2.

2.6. Microelectrode arrays

The development of spontaneous electrical activity in 8 and 15 wks differentiated cells was measured for 5 wks with a MEA system (Heikkilä et al., 2009). Recordings were obtained with an MEA60 amplifier and 60-6wellMEA200/30iR-Ti-w/o arrays with 9 electrodes per well (Multi Channel Systems [MCS], Reutlingen, Germany; Fig. 4A). A custom-made 6-well silicone chamber, SpikeBooster, was used to culture neural cells on MEA dishes as previously described (Kreutzer et al., 2012). The temperature was maintained at 37 °C with a TC02 temperature controller (MCS). Cultures were measured twice per week for 10 min, and the two weekly measurements were averaged for analysis (Supplementary Table 2, experimental repeats). The control of measurements and the detection of spikes were performed with MC_Rack software (MCS). A sampling rate of 50 kHz was used for the measurements. Spikes were detected from 200 Hz high-pass filtered data when their amplitude crossed the threshold of −5 × standard deviation (SD) of noise. Electrodes with a total spike frequency >0.033 Hz (2/min) were experimentally determined to present biological activity (*i.e.*, to be active electrodes; Supplementary Fig. 4A–C). The spike count and burst analysis were performed using a custom-made script for MATLAB (MathWorks, Natick, MA, USA) (Kapucu et al., 2012) with further modifications. Additional conditions were applied to the analysis to ensure the validity of burst detection: burst detection was only applied to channels where the total spike frequency was at least 0.167 Hz (10/min), and a minimum of three spikes was considered to form a burst. Furthermore, if the automatically detected burst inter-spike interval threshold exceeded 2000 ms, the channel was considered not to have bursts and was excluded from the burst analysis.

2.7. Statistical analysis

Due to the non-Gaussian distribution of the data, the non-parametric Kruskal Wallis test (with Dunn's *post hoc* – test) and Mann-Whitney *U* test were used. All the statistical tests were performed with SPSS Statistics software (version 23.0).

3. Results

3.1. hPCS differentiate efficiently into neuronal population with varying proportion of astrocytes

Using our simple neurosphere differentiation method (Lappalainen et al., 2010), we have tested the neural differentiation capacity of several hESC and hiPSC lines (Lappalainen et al., 2010; Toivonen et al., 2013) and have chosen the in-house derived hESC line Regea 08/023 and the hiPSC line 04311.WT for a detailed study of neuron and astrocyte differentiation and functionality (Fig. 1A). Cells were differentiated in suspension for either standard 8 week period or prolonged 15 week period and plated in adherent culture for maturation and experiments. For clarity, the names of the study's time points refer to both differentiation and maturation time points. For example, 8 + 2 wks refers to 8 weeks of differentiation in neurosphere culture, and 2 weeks of adherent maturation (Fig. 1A).

To examine the brain regional identity of the cells, we performed RT-PCR to 8 + 1 wk. samples and detected strong expression of forebrain (*FOXG1, OTX2*) and hindbrain (*GBX2*) markers, and minor expression of midbrain marker (*LMX1A*) (Fig. 1B). Expression of midbrain marker *EN1* and hindbrain marker *HOXA2* were not detected. RT-PCR analysis confirmed that the culture represents a mixed neural cell population.

In order to determine the differentiation capacity of the two hPSC lines, neuronal cells were immunostained with microtubule-associated protein 2 (MAP-2) and β-tubulin antibodies, and astrocytes with glial fibrillary acidic protein (GFAP) antibody. Quantification of the neuron-to-astrocyte ratio in the hESC line revealed good capacity to give rise to both neurons and astrocytes (Fig. 1C and D, for cell counts see Supplementary Fig. 2). Neuronal cells were efficiently produced, but their proportion was decreased with prolonged differentiation time from 73% at 8 + 4 wks to 44% at 15 + 4 wks (Fig. 1D). Astrocyte proportion increased gradually at the expense of neuronal cells from 2% at 8 + 4 wks to 51% at 15 + 4 wks (Fig. 1C and D). At the same time, proportion of cells without any neural staining was diminished from 25% at 8 + 4 wks to 5% at 15 + 4 wks. In line with the immunocytochemical data, the gene expression analysis revealed upregulation of astrocyte markers (*BLBP, GFAP, ALDH1L1, S100B, SLC1A3, SLC1A2,* and *GLUL*) after prolonged differentiation (15 + 5 wks) (Fig. 1F). Such robust changes

were not observed with neural precursor cell (NPC) markers (*PAX6, MSI2H*) or neuron markers (*NF68, NF200, RBFOX3, MAP2, SYN1*) (Fig. 1F).

The hiPSC line was shown to have a good capacity for neuronal differentiation but limited astrogenesis (Fig. 1C and E). The hiPSC line efficiently produced neuronal cells after standard differentiation time, and the proportion remained also high after prolonged differentiation: 80% at 8 + 4 wks and 70% at 15 + 4 wks (Fig. 1E). Contrary to the results obtained with hESC line, the increase in astrocyte proportion in hiPSC line was very modest, from 3% at 8 + 4 wks to 5% at 15 + 5 wks (Fig. 1E). The proportion of cells without any neural staining slightly increased from 17% at 8 + 4 wks to 25% at 15 + 4 wks. Furthermore, at the gene expression level, astrocyte markers were not upregulated in the hiPSC line (Fig. 1G). To summarize, these findings demonstrate that the hiPSC line (04311.WT) did not undergo astrocyte enrichment

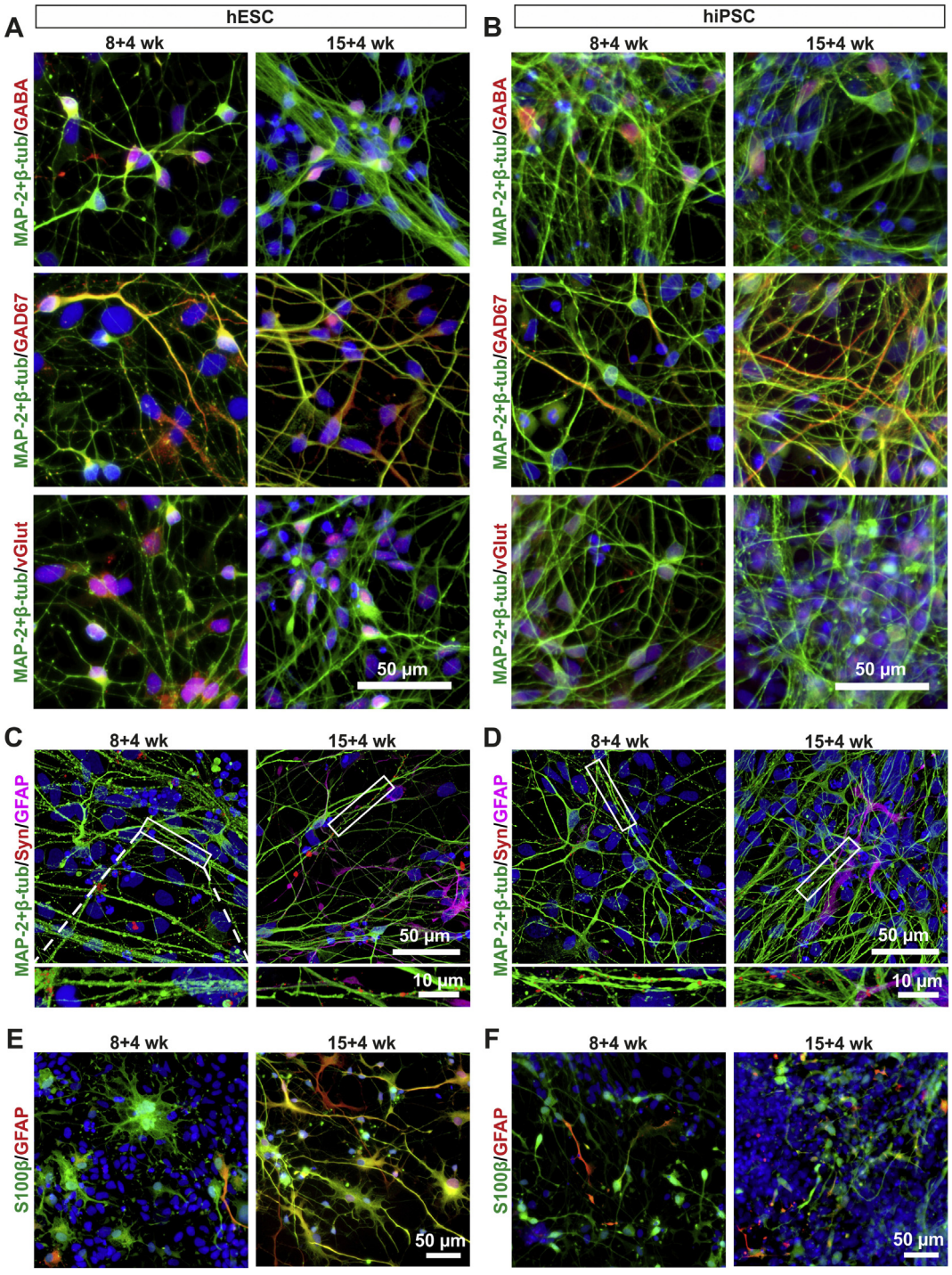

Fig. 2. Immunocytochemical characterization of neural cell types. Immunocytochemical staining verified specific neuronal subtypes expressing GABA, GAD67 and vGlut in both (A) hESC- and (B) hiPSC-derived 8 + 4 wks and 15 + 4 wks old cultures (n = 1). (C, D) Synaptophysin staining co-localized with the neuronal markers MAP-2 + β-tubulin in all analyzed cultures (*n* = 3). GFAP-positive astrocytes were sometimes found in close proximity to synaptophysin-positive neuronal processes after prolonged differentiation (15 + 4 wks). Insets below show a magnified view of synaptophysin staining along neuronal processes. (E, F) Astrocytes expressing the cell type-specific markers S100β and GFAP were found in all the cultures (n = 1). DAPI nuclear staining is shown in blue.

as efficiently as the hESC line (Regea 08/023). On the other hand, NPC and neuron markers were expressed at comparable level in both hPSC lines supporting overall good neuronal differentiation capacity.

3.2. Immunocytochemical characterization of hPSC-derived neural cultures

The majority of neurons were positive for GABAergic or glutamatergic markers in both 8 and 15 wk. differentiated cultures (Fig. 2A and B). Neurons expressing the presynaptic marker synaptophysin were detected at all the studied time points (Fig. 2C and D). Combined staining of synaptophysin with the neuronal markers revealed organized synaptophysin-positive boutons in neuronal processes. Occasionally, astrocyte processes were found aligned with synaptophysin-positive neuronal processes (Fig. 2C and D). Astrocytes were characterized with GFAP and S100 calcium-binding protein B (S100β) staining, and in most cases, both markers were co-localized (Fig. 2E and F). As stated earlier, the proportion of GFAP-positive astrocytes was increased after prolonged differentiation especially in the hESC line (Fig. 1) (Fig. 2E). Some astrocytes sent several-hundred-micrometer-long processes which often closely intertwined with neuronal axons and dendrites.

3.3. Prolonged differentiation enhances maturation of GABAergic system

To study the basic functional properties of the hESC- and hiPSC-derived neural cultures, we monitored intracellular Ca^{2+} dynamics using Fluo-4 AM dye (Fig. 3). First, we imaged spontaneous Ca^{2+} signaling and its blockage by tetrodotoxin (TTX). Next, γ-aminobutyric acid (GABA) and glutamate were applied to demonstrate for the presence of functional receptors for these major neurotransmitters. Finally, a high concentration of KCl was used to induce depolarization and voltage-gated Ca^{2+} channel activation. The subsequent immunocytochemical staining verified that Ca^{2+} signals were detected from both neurons and astrocytes (Fig. 3A–C). Examples of neuronal and astrocyte Ca^{2+} signals are presented in Supplementary Movies 1 and 2.

Spontaneous neuronal Ca^{2+} transients were detected at all the studied time points in both hPSC lines. Neurons exhibited Ca^{2+} events with single spikes and high-frequency oscillations (Fig. 3B and Movie 1). TTX reversibly blocked spontaneous Ca^{2+} signaling in a subset of neurons (Fig. 3B), indicating that the activation of Na^{+} voltage-gated channels due to depolarization is a critical step for spontaneous, action potential-related Ca^{2+} signaling in neuronal cells (Fig. 3E and F).

Responses to GABA and glutamate application confirmed the presence of functional receptor-operated channels in neurons. Glutamate induced an instant, strong Ca^{2+} elevation in the majority (85–99%) of the analyzed neurons (Fig. 3G and H). The amplitudes of the glutamate responses are presented in Supplementary Fig. 3A. In contrast to glutamate treatment, the neuronal responses to GABA application varied considerably between studied time points. In most cases, GABA had an excitatory effect increasing intracellular Ca^{2+} (Fig. 3B) but occasionally spontaneous activity of neurons was attenuated by GABA treatment (Fig. 3D). In the hESC line, the proportion of neurons responding to GABA with a Ca^{2+} rise (excitatory action) decreased progressively during both prolonged differentiation and adherent maturation. GABA response decreased from 76% at 8 + 2 wks to 24% at 15 + 4 wks (Fig. 3I). The reduction in excitatory GABA response over time was not as prominent in the hiPSC line as in the hESC line. In hiPSC line, proportion of GABA-responsive cells decreased from 61% at 8 + 2 wks to 51% at 15 + 4 wks (Fig. 3J). The changes in GABA response amplitudes are presented in Supplementary Fig. 3C and D. To support these results we performed RT-PCR analysis of chloride transporter genes *NKCC1* and *KCC2*, important for the developmental change of GABA response from excitatory to inhibitory (Ben-Ari et al., 2012). In both hPSC lines, the expression of *NKCC1*, a marker of early development, was strongest in 8 + 1 wk. time point after which it was down-regulated (Fig. 3K). *KCC2* expression, which starts later in development, was observed at 15 + 1 wk. time point (Fig. 3K).

All in all, both of the studied hPSC lines demonstrated similar trends in the development of pharmacological responses over time. Maturation of GABAergic system was observed as a result of prolonged differentiation.

3.4. Prolonged differentiation promotes maturation of spontaneous activity

Spontaneous electrical activity in neuronal cultures was measured using MEA (Fig. 4A and B) as previously described (Heikkilä et al., 2009). Significant differences between hPSC lines, as well as numerical details (medians and averages) are presented in Supplementary Table 3. To verify the dependency of activity on excitatory and inhibitory synaptic factors, we used a pharmacological test battery containing N-Methyl-D-aspartate (NMDA), α-amino-3-hydroxy-5-methyl-4-isoxazolepropionic acid (AMPA)/kainate and GABA receptor ligands (Supplementary Fig. 4).

The hESC-derived cultures followed an activity development curve after standard differentiation with a high-activity peak at 8 + 3 and 8 + 4 wks (Fig. 4C, E and G). Similar clear curves were not detected in the hiPSC-derived cultures after standard differentiation (8+ wks; Fig. 4D, F and H) or from either of the hPSC lines after prolonged differentiation (15+ wks; Fig. 4C–H). All in all, there were more active electrodes in the hESC-derived cultures, and prolonged differentiation significantly reduced the proportion of active electrodes per culture with both hPSC lines (Supplementary Table 2 and Fig. 4C and D).

Spike frequency in active electrodes is a frequently used measure of neuronal activity (Fukushima et al., 2016). The median and average spike frequency values are listed in Supplementary Table 3 (see also Supplementary Movie 3). In the hESC-derived cultures, the spike frequency reached a maximum during the high-activity peak at 8 + 4 wks, with a median value of 0.276 Hz (Fig. 4E). At the corresponding time point after prolonged differentiation (15 + 4 wks), the spike frequency was significantly reduced to 0.132 Hz ($p = 0.020$). Similar reductions in spike frequency were observed with the hiPSC-derived cultures (Fig. 4F).

Spontaneous bursts were detected in all the studied groups (Fig. 4C and D). Prolonged differentiation (15+ wks) significantly reduced the proportion of burst-detecting electrodes (Fig. 4C and D). Nonetheless, in those burst-detecting electrodes, burst counts increased significantly in both hPSC lines (Fig. 4G and H). In the hESC line, the greatest increase in burst number was detected between 8 + 2 and 15 + 2 wks, from 30 to 81 bursts per electrode ($p = 0.012$). In the hiPSC line, the highest increase was already between 8 + 1 and 15 + 1 wks, from 25 to 80 bursts per electrode ($p = 0.046$).

According to these results, prolonged differentiation affected the organization neuronal activity similarly in both hPSC lines by condensing the activity to fewer electrodes, which in turn expressed more frequent burst activity. The spike frequency and burst counts in active electrodes were similar between the hPSC lines verifying that the level of activity development was comparable.

3.5. Prolonged differentiation affects burst characteristics

After concluding that both hPCS lines develop similar bursting activity, we next studied in detail the basic burst characteristics: spike frequency in bursts, burst duration and number of spikes per burst (Fig. 5). Numerical details (median and mean values) of burst parameters and significant differences between the hPSC lines are presented in Supplementary Table 4. Prolonged differentiation (15+ wks) of the hESC-derived cultures significantly increased the spike frequency in bursts at 4 out of 5 time points (Fig. 5A). The difference was most notable between 8 + 3 and 15 + 3 wks, with median frequency values of 11 Hz and 25 Hz ($p < 0.001$). In contrast, in the hiPSC line, spike frequency in bursts was reduced as result of prolonged differentiation. This reduction was most evident between 8 + 3 and 15 + 3 wks, when the median values were 19 Hz and 5 Hz ($p = 0.002$, Fig. 5B).

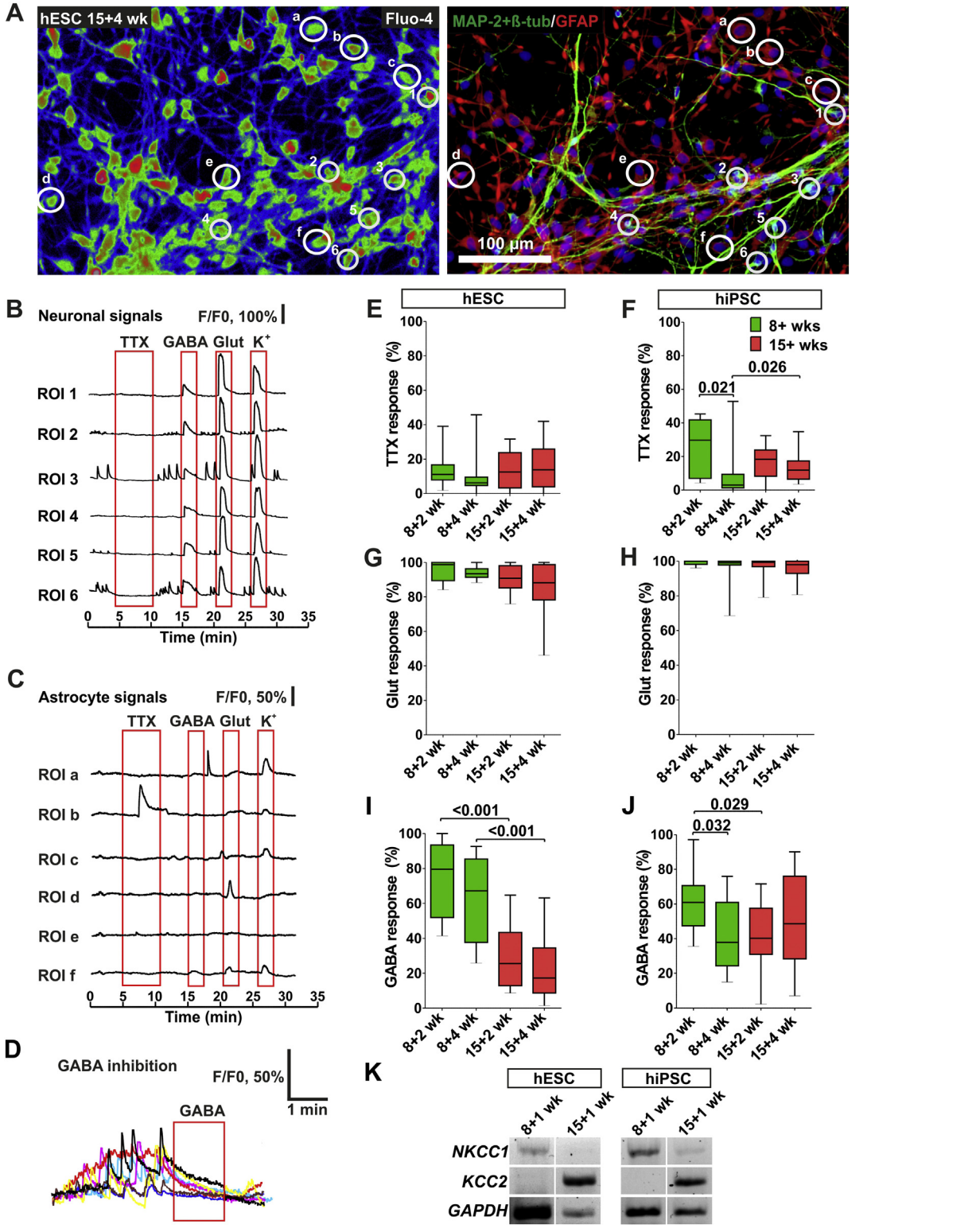

Fig. 3. Ca^{2+} signaling after standard and prolonged differentiation. (A) For calcium imaging experiments neural culture was loaded with Fluo-4 AM Ca^{2+} indicator. On the left a representative pseudocolor image of Fluo-4 loaded culture where red indicates high and blue indicates low Ca^{2+} levels. On the right is the same field after immunocytochemical staining of neuronal cells (MAP-2 + β-tubulin) and astrocytes (GFAP). DAPI nuclear staining is in blue. Neurons are marked with small region of interest (ROI) and numbering, and astrocytes are marked with large ROI and letters. Typical traces of (B) neuronal and (C) astrocyte Ca^{2+} signals. (D) Example traces showing attenuation of spontaneous neuronal Ca^{2+} signaling by GABA. Cultures showed both spontaneous activity and responses to pharmacological treatments. (E, F) Percentages of neuronal cells silenced by TTX (1 µM) treatment after standard and prolonged differentiation. Percentage of neuronal cells responding to (G, H) glutamate (Glut, 50 µM) and (I, J) GABA (100 µM) applications. The data are presented as the distribution of the percentages at each time point. The median and interquartile ranges are indicated by lines, and the whiskers indicate the minimum and maximum of the data. A non-parametric Mann-Whitney *U* test was used for the statistical analysis, and p-values <0.05 were considered significant. Significant p-values are presented in the images. See also Supplementary Fig. 3 for response amplitudes. The number of samples analyzed is presented in Supplementary Table 2. For all analyses (*E*-J), cells with neuronal morphology responding to high K^+ application were included. (K) The expression of chloride channel genes *NKCC1* and *KCC2* was determined with RT-PCR in both cell lines at 8 + 1 and 15 + 1 wk. time points (n = 1). The RT-PCR products from the two hPSC lines were analyzed on separate gels and image exposure times for the two gels were identical. Otherwise the bands representing different genes and time points were cropped from a single image of one gel (Supplementary Fig. 5B and C).

Burst duration was significantly reduced by prolonged differentiation (15+ wks) at 4 out of 5 time points in the hESC-derived cultures (Fig. 5C). The difference was most prominent between 8 + 3 wks and 15 + 3 wks, with median values of 476 ms and 223 ms ($p < 0.001$). In the hiPSC-derived cultures, however, prolonged differentiation increased the burst duration; the median duration was 286 ms at 8 + 3 wks and 1883 ms at 15 + 3 wks ($p = 0.001$, Fig. 5D). The number of spikes per burst was unaffected in most time points (medians between 4 and 6; Fig. 5E and F). Almost all the significant changes in spike frequency in burst and burst duration occurred at the same time points (Fig. 5A and B *vs.* C and D). Therefore, it appears that changes in burst duration were responsible for the differences in spike frequency in bursts.

To summarize, after prolonged differentiation the hESC-derived cultures demonstrated increased spike frequency in bursts, which was associated with reduced burst duration. Prolonged differentiation did not support similar burst development in the hiPSC-derived cultures.

4. Discussion

In our culture system, prolonged differentiation resulted in a switch from neurogenesis to astrogenesis recapitulating the *in vivo* developmental stages, as previously described (Itsykson et al., 2005; Nat et al., 2007). We characterized the effects of prolonged differentiation on cell type composition, and studied neuronal function using Ca^{2+} imaging and MEA. Here, we report that prolonged neuronal differentiation enhances the functional maturation of hPSC-derived neuronal cultures.

Propensity for astrogenesis varied substantially between the studied hPSC lines in long-term follow-up. The neuron-to-astrocyte ratio was similar in both hPSC lines after standard 8 weeks of differentiation but after prolonged 15 weeks of differentiation, the ratio was strikingly different. The astrocyte proportion in the hiPSC line was very modest, only 5%, whereas the hESC line produced up to 50% of astrocytes. Earlier studies also showed variation in neuron and astrocyte differentiation among hPSC lines regardless of their origin (Emdad et al., 2012; Toivonen et al., 2013). Especially in hiPSC lines, incomplete transgene silencing and epigenetic differences can affect differentiation capacity (Hatada et al., 2008; Kim et al., 2010). Although pluripotency-inducing transgenes were silenced in the hiPSC line used in the present work, possible methylation of astrocyte-specific genes might delay astrocyte differentiation (Hatada et al., 2008; Majumder et al., 2013). Generally, differentiation capacity is known to be related to intrinsic properties of the particular hPSC line (Emdad et al., 2012; Hu et al., 2010; Toivonen et al., 2013).

The neuronal cells produced a mixed population of glutamatergic neurons with a subset of GABAergic neurons, as demonstrated by immunocytochemistry and functional measurements. These results are in line with a recent report characterizing the generation of glutamatergic and GABAergic neurons from hPSCs using another neurosphere differentiation protocol (Floruta et al., 2017). Here, both hPSC lines showed similar properties respective to action potential generation and glutamate responsiveness. hPSC-derived neurons also responded at comparative levels to high K^+ and glutamate applications similarly as previously described by Forostyak et al. (2013). After standard 8 weeks differentiation, our GABAergic population was immature and responded to GABA application with excitation. Also, we detected expression of chloride transporter *NKCC1*, which is prominently expressed in early GABAergic development (Ben-Ari et al., 2012). During prolonged differentiation, we observed a typical reduction in the excitatory GABAergic response and concurrent increase chloride transporter *KCC2*, a mature marker for chloride transporter development (Ben-Ari et al., 2012). Together these changes imply developmental maturation of the GABAergic system as a result of prolonged differentiation.

MEA experiments showed that spontaneous neuronal activity could be repeatedly measured from all the studied time points. The analysis revealed varying electrical activity patterns, resulting in a non-Gaussian distribution of the data. A very comprehensive, large-scale study by Wagenaar and colleagues showed similar MEA data distribution with rodent primary neuronal networks (Wagenaar et al., 2006). Although MEA studies with rodent-derived neuronal cultures provide a well-established reference for future applications, even primary human and primary rodent cultures are far from comparable. Human cultures tend to have a significantly slower rate of activity development, lower percentage of active electrodes and spike counts in comparison to rodent cultures (Napoli and Obeid, 2016). The current results show that also human stem cell-derived cultures have a comparatively low percentage of active electrodes and low spike counts. Therefore the characteristics of hPSC-derived cultures need to be considered in MEA experimental design, execution and data analysis.

MEA analysis revealed that prolonged differentiation decreased the overall spike frequency and condensed electrical activity to particular areas in the culture. Although the overall level of activity seemed to decrease in prolonged differentiation, the remaining activity organized from single spikes into bursts with increasing bursting frequency. As bursts are thought to represent more mature neuronal function, the increase in burst number after prolonged differentiation should be expected. The observed reduction in the percentage of active and burst detecting electrodes could be attributed to synaptic pruning (Yamamoto and López-Bendito, 2012; Benders et al., 2015) or the increase in proportion of astrocytes at the expense of neurons after prolonged differentiation. Even though, the amount of spontaneous spike and burst activity was in a comparable level between the studied hPSC lines after prolonged differentiation, closer analysis revealed differences in their activity patterns. In the hESC line prolonged differentiation was associated with burst compaction. Mature compact bursts were not formed similarly in the hiPSC line. This, and the slight increase of non-neuronal and non-astrocytic cells in the hiPSC line after prolonged differentiation may reflect aberrant differentiation, which supports the observation that not all cell lines mature as efficiently after extended culture times (Emdad et al., 2012; Toivonen et al., 2013). Also, the studied hESC line produced a substantial amount of endogenous astrocytes (>50%) which could partly help in stabilizing neuronal activity and support compaction of burst activity in long-term culture. However, dissecting these processes pharmacologically in astrocytes alone is very challenging, and new approaches are needed to address these questions. Even though hPSC-derived neuron cocultures with rodent astrocytes are relatively well established, the cocultures with human astrocytes need to be better validated.

In conclusion, we found that the studied hPSC lines underwent neurogenic-to-gliogenic switch during prolonged differentiation. However, there were striking differences in the efficiency of astrogenesis which should be considered also more carefully in the field. Despite its challenges, prolonged neural differentiation induces functional changes which mimic the development occurring *in vivo*, and in the future it can be utilized in development of more representative hPSC-derived neural models.

Supplementary data to this article can be found online at https://doi.org/10.1016/j.scr.2018.01.018.

Author contributions

S.N., T.P., A.P. and D.F. designed the study; T.P., A.P., D.F. and M.P. performed experiments; M.M. contributed new analytic tools; T.P., A.P. and D.F. analyzed data; H.H. assisted with the statistical analysis; and T.P., A.P. and S.N. wrote the paper. T.P. and A.P. contributed equally to this work. All authors edited the article.

Competing financial interests

Authors declare no competing financial interests.

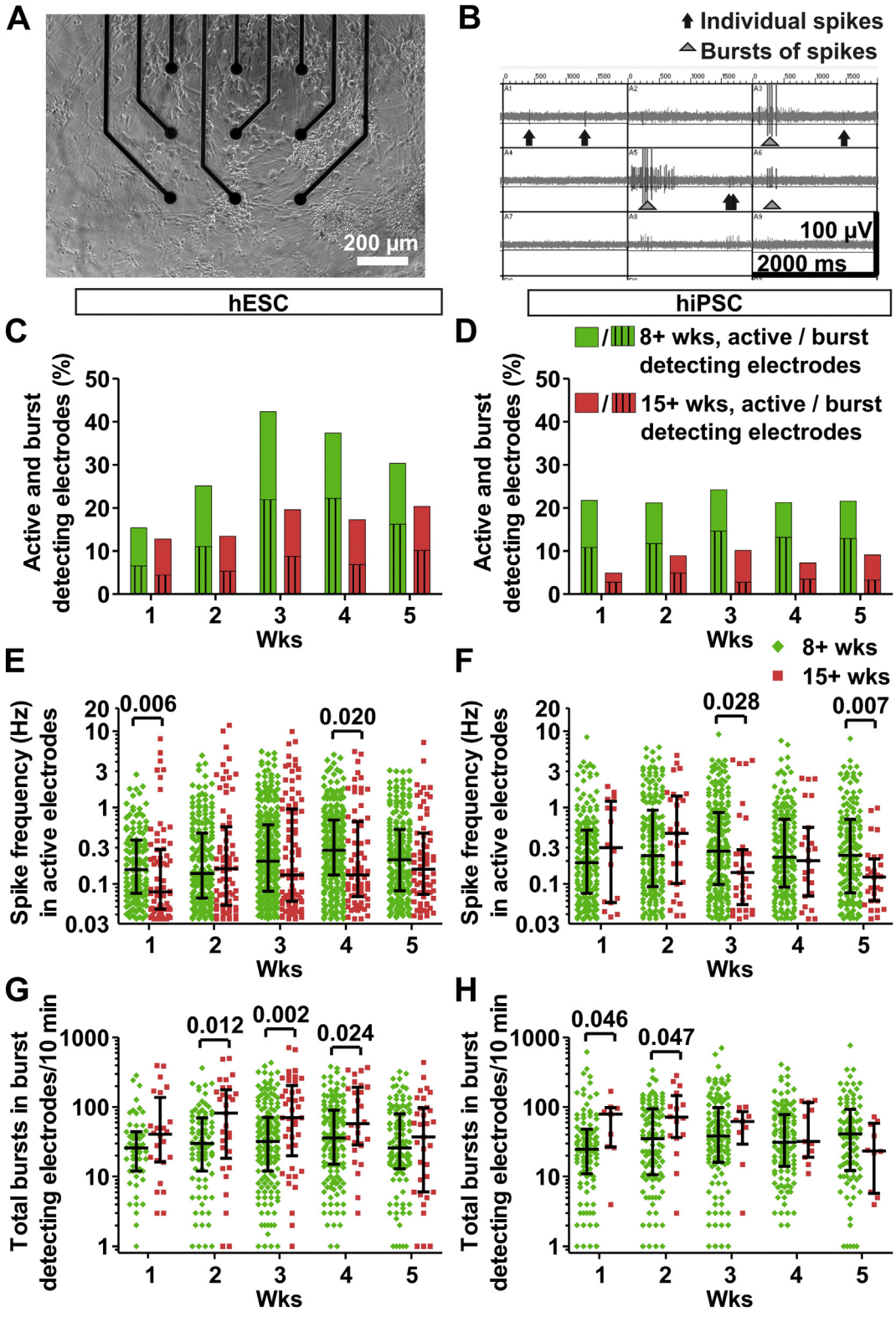

Fig. 4. Spike and burst activity development after standard and prolonged differentiation. (A) Activity was measured with 9 electrodes per well. (B) Spikes were detected when their amplitude exceeded a threshold of 5 × standard deviation of background noise. Vertical scale bar is 100 µV and horizontal 2 s. (C, D) The percentage of active (colored bars, no texture) and burst detecting electrodes (colored bars, striped) was calculated from spike and burst counts determined using a custom-made MATLAB algorithm. (E, F) The spike frequency in active electrodes was calculated from the same data. (G, H) The number of bursts in burst-detecting electrodes was also calculated. The numbers of spikes and bursts (E-H) are presented as scatter plots on a logarithmic scale; each dot represents a single electrode, the horizontal line indicates the median, and whiskers indicate the interquartile range. See also Supplementary Table 3. The numbers of analyzed cultures and electrodes are presented in Supplementary Table 2. Statistical significance was calculated using the Mann-Whitney U test, and a p-value <0.05 was considered significant. Significant p-values are presented in the images.

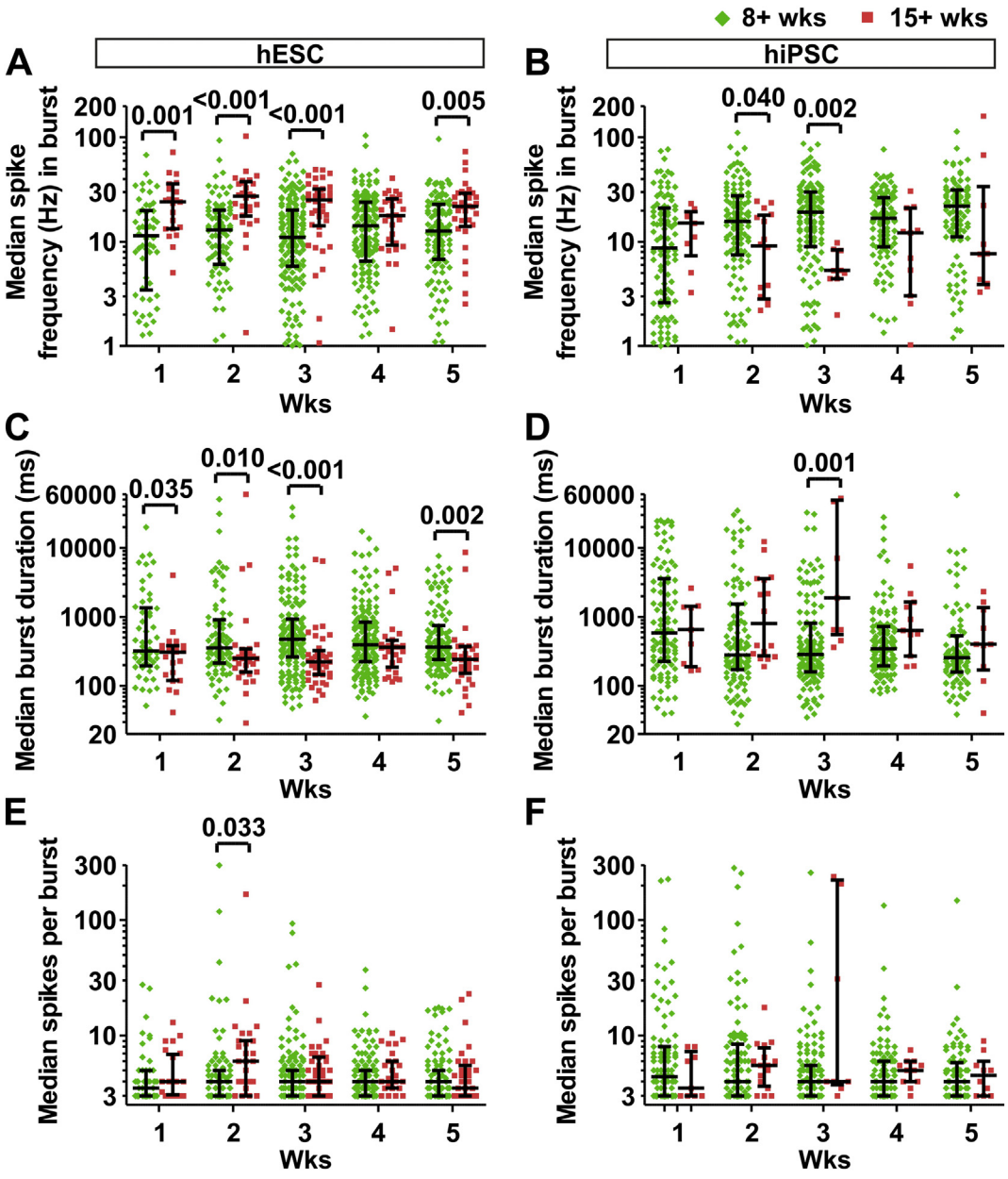

Fig. 5. Burst parameters after standard and prolonged differentiation. (A, B) MEA data were analyzed with a custom-made MATLAB script to determine the spike frequency in bursts. (C, D) Burst duration was also calculated. (E, F) The number of spikes per burst was determined. Each dot in the scatter plot represents the median result from a single electrode on a logarithmic scale. The median and interquartile range are indicated by the line and whiskers, respectively. See also Supplementary Table 4. The numbers of analyzed cultures and electrodes are presented in Supplementary Table 2. Due to high variation in the data, a small number of data points are outside the axis limits (A: 13; B: 4; C: 7; D: 8; E: 3; F: 4; see Supplementary Table 4 for the full range of results). Statistical significances between groups were calculated using the Mann-Whitney U test and significant p-values (<0.05) are indicated in the figure.

Acknowledgements

The authors thank the iPS Cells Facility, University of Tampere, for providing the undifferentiated hiPSCs and Hanna Mäkelä and Eija Hannuksela for technical assistance with cell maintenance and molecular biology analyses. We thank the Imaging Facility and Facility of Electrophysiological Measurements, University of Tampere, and especially Juha Heikkilä and Marco Fabiani for technical assistance with the MEA measurements. We also thank Dr. Laura Ylä-Outinen, PhD, for her advice and constructive criticism throughout the project. This work was supported by the 3DNeuroN project in the European Union's Seventh Framework Programme, Future and Emerging Technologies, grant agreement n°296590. It was also supported by the Human Spare Parts 2 program, The Finnish Funding Agency for Innovation, TEKES. T.P. received support from the Tampere City Science Foundation and Alfred Kordelin Foundation, and A.P. from the Juliana von Wendt Fund.

References

Ben-Ari, Y., Khalilov, I., Kahle, K.T., Cherubini, E., 2012. The GABA excitatory/inhibitory shift in brain maturation and neurological disorders. Neuroscientist 18, 467–486.

Benders, M.J., Palmu, K., Menache, C., Borradori-Tolsa, C., Lazeyras, F., Dubois, J., Vanhatalo, S., Huppi, P.S., 2015. Early Brain Activity Relates to Subsequent Brain Growth in Premature Infants. Cereb. Cortex 25, 3014–3024.

Carpenter, A.E., Jones, T.R., Lamprecht, M.R., Clarke, C., Kang, I.H., Friman, O., Guertin, D.A., Chang, J.H., Lindquist, R.A., Moffat, J., Golland, P., Sabatini, D.M., 2006. CellProfiler: image analysis software for identifying and quantifying cell phenotypes. Genome Biol. 7.

Clarke, L.E., Barres, B.A., 2013. Emerging roles of astrocytes in neural circuit development. Nat. Rev. Neurosci. 14, 311–321.

Du, X., Parent, J.M., 2015. Using patient-derived induced pluripotent stem cells to model and treat epilepsies. Curr. Neurol. Neurosci. Rep. 15.

Emdad, L., D'Souza, S.L., Kothari, H.P., Qadeer, Z.A., Germano, I.M., 2012. Efficient differentiation of human embryonic and induced pluripotent stem cells into functional astrocytes. Stem Cells Dev. 21, 404–410.

Floruta, C.M., Du, R., Kang, H., Stein, J.L., Weick, J.P., 2017. Default patterning produces pan-cortical glutamatergic and CGE/LGE-like GABAergic neurons from human pluripotent stem cells. Stem Cell Rep. 9, 1463–1476.

Forostyak, O., Romanyuk, N., Verkhratsky, A., Sykova, E., Dayanithi, G., 2013. Plasticity of calcium signaling cascades in human embryonic stem cell-derived neural precursors. Stem Cells Dev. 22, 1506–1521.

Frega, M., van Gestel, S.H., Linda, K., van der Raadt, J., Keller, J., Van Rhijn, J.R., Schubert, D., Albers, C.A., Nadif Kasri, N., 2017. Rapid neuronal differentiation of induced pluripotent stem cells for measuring network activity on micro-electrode arrays. J. Vis. Exp. 119.

Fukushima, K., Miura, Y., Sawada, K., Yamazaki, K., Ito, M., 2016. Establishment of a human neuronal network assessment system by using a human neuron/astrocyte co-culture derived from fetal neural stem/progenitor cells. J. Biomol. Screen. 21, 54–64.

Hatada, I., Namihira, M., Morita, S., Kimura, M., Horii, T., Nakashima, K., 2008. Astrocyte-specific genes are generally demethylated in neural precursor cells prior to astrocytic differentiation. PLoS One 3, e3189.

Heikkilä, T.J., Ylä-Outinen, L., Tanskanen, J.M.A., Lappalainen, R.S., Skottman, H., Suuronen, R., Mikkonen, J.E., Hyttinen, J.A.K., Narkilahti, S., 2009. Human embryonic stem cell-derived neuronal cells form spontaneously active neuronal networks in vitro. Exp. Neurol. 218, 109–116.

Hu, B., Weick, J.P., Yu, J., Ma, L., Zhang, X., Thomson, J.A., Zhang, S., 2010. Neural differentiation of human induced pluripotent stem cells follows developmental principles but with variable potency. Proc. Natl. Acad. Sci. U. S. A. 107, 4335–4340.

Itsykson, P., Ilouz, N., Turetsky, T., Goldstein, R.S., Pera, M.F., Fishbein, I., Segal, M., Reubinoff, B.E., 2005. Derivation of neural precursors from human embryonic stem cells in the presence of noggin. Mol. Cell. Neurosci. 30, 24–36.

Johnson, M.A., Weick, J.P., Pearce, R.A., Zhang, S.-., 2007. Functional neural development from human embryonic stem cells: accelerated synaptic activity via astrocyte coculture. J. Neurosci. 27, 3069–3077.

Johnstone, A.F.M., Gross, G.W., Weiss, D.G., Schroeder, O.H., Gramowski, A., Shafer, T.J., 2010. Microelectrode arrays: a physiologically based neurotoxicity testing platform for the 21st century. Neurotoxicology 31, 331–350.

Jones, T.R., Kang, I.H., Wheeler, D.B., Lindquist, R.A., Papallo, A., Sabatini, D.M., Golland, P., Carpenter, A.E., 2008. CellProfiler Analyst: data exploration and analysis software for complex image-based screens. BMC Bioinform. 9.

Kapucu, F.E., Tanskanen, J.M.A., Mikkonen, J., Ylä-Outinen, L., Narkilahti, S., Hyttinen, J.A.K., 2012. Burst analysis tool for developing neuronal networks exhibiting highly varying action potential dynamics. Front. Comput. Neurosci. 6.

Kim, K., Doi, A., Wen, B., Ng, K., Zhao, R., Cahan, P., Kim, J., Aryee, M.J., Ji, H., Ehrlich, L.I.R., Yabuuchi, A., Takeuchi, A., Cunniff, K.C., Hongguang, H., McKinney-Freeman, S., Naveiras, O., Yoon, T.J., Irizarry, R.A., Jung, N., Seita, J., Hanna, J., Murakami, P., Jaenisch, R., Weissleder, R., Orkin, S.H., Weissman, I.L., Feinberg, A.P., Daley, G.Q., 2010. Epigenetic memory in induced pluripotent stem cells. Nature 467, 285–290.

Kreutzer, J., Ylä-Outinen, L., Kärnä, P., Kaarela, T., Mikkonen, J., Skottman, H., Narkilahti, S., Kallio, P., 2012. Structured PDMS chambers for enhanced human neuronal cell activity on MEA platforms. J. Bionic Eng. 9.

Lappalainen, R.S., Salomäki, M., Ylä-Outinen, L., Heikkilä, T.J., Hyttinen, J.A., Pihlajamäki, H., Suuronen, R., Skottman, H., Narkilahti, S., 2010. Similarly derived and cultured hESC lines show variation in their developmental potential towards neuronal cells in long-term culture. Regen. Med. 5, 749–762.

Li, K., Javed, E., Scura, D., Hala, T.J., Seetharam, S., Falnikar, A., Richard, J., Chorath, A., Maragakis, N.J., Wright, M.C., Lepore, A.C., 2015. Human iPS cell-derived astrocyte transplants preserve respiratory function after spinal cord injury. Exp. Neurol. 271, 479–492.

Lindvall, O., 2015. Treatment of Parkinson's disease using cell transplantation. Philos. Trans. R. Soc. B Biol. Sci. 370, 20140370.

Majumder, A., Dhara, S.K., Swetenburg, R., Mithani, M., Cao, K., Medrzycki, M., Fan, Y., Stice, S.L., 2013. Inhibition of DNA methyltransferases and histone deacetylases induces astrocytic differentiation of neural progenitors. Stem Cell Res. 11, 574–586.

Miller, F.D., Gauthier, A.S., 2007. Timing is everything: making neurons versus glia in the developing cortex. Neuron 54, 357–369.

Napoli, A., Obeid, I., 2016. Comparative analysis of human and rodent brain primary neuronal culture spontaneous activity using micro-electrode array technology. J. Cell. Biochem. 117, 559–565.

Nat, R., Nilbratt, M., Narkilahti, S., Winblad, B., Hovatta, O., Nordberg, A., 2007. Neurogenic neuroepithelial and radial glial cells generated from six human embryonic stem cell lines in serum-free suspension and adherent cultures. Glia 55, 385–399.

Odawara, A., Saitoh, Y., Alhebshi, A.H., Gotoh, M., Suzuki, I., 2014. Long-term electrophysiological activity and pharmacological response of a human induced pluripotent stem cell-derived neuron and astrocyte co-culture. Biochem. Biophys. Res. Commun. 443, 1176–1181.

Ojala, M., Prajapati, C., Pölönen, R., Rajala, K., Pekkanen-Mattila, M., Rasku, J., Larsson, K., Aalto-Setälä, K., 2016. Mutation-specific phenotypes in hiPSC-derived cardiomyocytes carrying either myosin-binding protein C or α-tropomyosin mutation for hypertrophic cardiomyopathy. Stem Cells Int. 2016, 1684792.

Pasca, A.M., Sloan, S.A., Clarke, L.E., Tian, Y., Makinson, C.D., Huber, N., Kim, C.H., Park, J., O'Rourke, N.A., Nguyen, K.D., Smith, S.J., Huguenard, J.R., Geschwind, D.H., Barres, B. A., Pasca, S.P., 2015. Functional cortical neurons and astrocytes from human pluripotent stem cells in 3D culture. Nat. Methods 12, 671–678.

Rajala, K., Hakala, H., Panula, S., Aivio, S., Pihlajamäki, H., Suuronen, R., Hovatta, O., Skottman, H., 2007. Testing of nine different xeno-free culture media for human embryonic stem cell cultures. Hum. Reprod. 22, 1231–1238.

Rajala, K., Lindroos, B., Hussein, S.M., Lappalainen, R.S., Pekkanen-Mattila, M., Inzunza, J., Rozell, B., Miettinen, S., Narkilahti, S., Kerkelä, E., Aalto-Setälä, K., Otonkoski, T., Suuronen, R., Hovatta, O., Skottman, H., 2010. A defined and xeno-free culture method enabling the establishment of clinical-grade human embryonic, induced pluripotent and adipose stem cells. PLoS One 5, e10246.

Shi, Y., Kirwan, P., Smith, J., Robinson, H.P.C., Livesey, F.J., 2012. Human cerebral cortex development from pluripotent stem cells to functional excitatory synapses. Nat. Neurosci. 15 (477-U180).

Skottman, H., 2010. Derivation and characterization of three new human embryonic stem cell lines in Finland. In Vitro Cell. Dev. Biol. Anim. 46, 206–209.

Suzuki, I.K., Vanderhaeghen, P., 2015. Is this a brain which I see before me? Modeling human neural development with pluripotent stem cells. Development 142, 3138–3150.

Takahashi, K., Tanabe, K., Ohnuki, M., Narita, M., Ichisaka, T., Tomoda, K., Yamanaka, S., 2007. Induction of pluripotent stem cells from adult human fibroblasts by defined factors. Cell 131, 861–872.

Thomson, J.A., 1998. Embryonic stem cell lines derived from human blastocysts. Science 282, 1145–1147.

Toivonen, S., Ojala, M., Hyysalo, A., Ilmarinen, T., Rajala, K., Pekkanen-Mattila, M., Äänismaa, R., Lundin, K., Palgi, J., Weltner, J., Trokovic, R., Silvennoinen, O., Skottman, H., Narkilahti, S., Aalto-Setälä, K., Otonkoski, T., 2013. Comparative analysis of targeted differentiation of human induced pluripotent stem cells (hiPSCs) and human embryonic stem cells reveals variability associated with incomplete transgene silencing in retrovirally derived hiPSCs lines. Stem Cells Transl. Med. 2, 83–93.

Wagenaar, D.A., Pine, J., Potter, S.M, 2006. An extremely rich repertoire of burstingpatterns during the development of cortical cultures. BMC Neurosci. 7.

Yamamoto, N., López-Bendito, G., 2012. Shaping brainconnections through spontaneous neural activity. Eur. J. Neurosci. 35, 1595–1604.

Ylä-Outinen, L., Heikkilä, J., Skottman, H., Suuronen, R., Äänismaa, R., Narkilahti, S., 2010. Human cell-based micro electrode array platform for studying neurotoxicity. Front. Neuroeng. 3.

Zhang, S., Wernig, M., Duncan, I.D., Brüstle, O., Thomson, J.A., 2001. In vitro differentiation of transplantable neural precursors from human embryonic stem cells. Nat. Biotechnol. 19, 1129–1133.